Microchip-based electrokinetic biosensor: microfabrication and application in membrane protein profiling of extracellular vesicles

Moein Talebian Gevari [1, *], Siddharth Sourabh Sahu [2], Dhrubaditya Mitra [3], Petra Hååg [4], Kristina Viktorsson [4], Shili Zhang [1], Jan Linnros [2], and Apurba Dev [1, 2, *]

[1] Department of Electrical Engineering, The Ångström Laboratory, Uppsala University, 75121 Uppsala, Sweden.

[2] Department of Applied Physics, School of Engineering Sciences, KTH Royal Institute of Technology, 10691 Stockholm, Sweden.

[3] NORDITA, KTH Royal Institute of Technology and Stockholm University, 10691 Stockholm, Sweden.

[4] Department of Oncology-Pathology, Karolinska Institutet, S-171 64, Solna, Sweden.

[*] Corresponding author

E-mail address: apurba.dev@angstrom.uu.se (A. Dev), moein.talebian@angstrom.uu.se (M.T. Gevari).

Abstract

In this study, we demonstrate the fabrication, characterization, and application of a microchip-based electrokinetic biosensor which exploits streaming current for signal transduction. The sensor chips, fabricated using standard silicon fabrication techniques, are based on Si-glass microfluidics offering precision, robustness, and transparency. A custom-built chip-manifold allowing easy interfacing with standard microfluidic connections is also developed which shows leak-free integration of the microchips up to 6 bar of applied pressure. Within this range of pressure, the devices show linear and highly reproducible values for flow rates and streaming current with RMS noise below 20 pA. The microchips designed for multiplexed measurements were tested with the detection of free proteins (streptavidin) and also transmembrane proteins of small extracellular vesicles (sEVs) to demonstrate the capacity of the microchips to detect various types of bio-analytes. The limit of detection (LOD) for streptavidin was estimated to be 0.5 nM while for the transmembrane protein (CD9), the LOD was found to be 1.2×10^{6} sEVs/mL. The sensitivity (LOD) of the devices was found to be about 4 times better in targeting CD9 transmembrane protein of H1975 extracellular vesicles when compared to commercial silica capillary which was used previously. The improvement in LOD is attributed to the

higher surface quality of the sensor in terms of the density of surface charges which may be further exploited for even lower LOD. In addition, optical detection of fluorophore-tagged standard proteins was done through the optical window of the chip manifold and the transparent glass cap of the microchip.

Keywords: *Streaming current, microchip biosensor, Extracellular Vesicles, Microfluidics, Electrokinetics*

1. Introduction

During the past years, the principle of electrokinetic-biosensor exploiting streaming current/potential method has been applied in the detection of a wide variety of bio-analytes including proteins [1, 2], ligands [3], DNA [4] and extracellular vesicles [5], thereby demonstrating the excellent potential of the method as a generic biosensor. The method relies on the electrostatic and hydrodynamic interaction at the solid-liquid interface inside a microfluidic channel and allows for label-free detection of bio-analytes. A major benefit of the method stems from its high sensitivity to the surface coverage of an analyte, which has been previously studied with respect to its influence on the streaming current [6] and lately, for the determination of concentration of bio-analytes [7]. Besides, the method offers several practical benefits, such as low sample consumption, simple and inexpensive device architecture, and possibility to integrate with standard microfluidic technologies for sample sorting, enrichment, and deliveries. These advantages have obviously attracted further interest in the method aiming for both improved understanding and exploitation of the governing principles. In particular, we have recently demonstrated that the surface charge density and the charge contrast between the sensor surface and analyte play a major role which can be exploited to achieve a far better sensitivity [8, 9]. Further, by designing appropriate charge-labelled detection probe, we demonstrated the possibility to develop an immunosandwich assay in electrokinetic sensing, thereby, extending the application of the method in complex biofluid [8]. A multiplexed detection setup for simultaneous measurement of several bio-analytes has also been reported [10].

52 Clearly, the detection principle has matured in its ability to analyze bio-analytes, significantly
53 improving in both sensitivity and specificity. An improved understanding of how the physical
54 parameters of an analyte, such as its size and charge, influence the sensor response [11] now provides
55 us new opportunities to design a more sensitive detector. However, the developments so far have mainly
56 been shown using commercial silica capillary, which has limited scope to exploit many of the benefits
57 in practical settings. Instead, an implementation of the detection principle on a microfabricated channels
58 can help to further leverage some of the key advantages of the method. This includes the design of
59 shorter and narrower channels to further reduce sample consumption, improving the quality of surface
60 oxides for better sensitivity and integration of large number of channels for improving the throughput
61 of multiplexing. In addition, such a microfabricated sensor can open new avenues for research, e.g.,
62 new material for sensing surface, integration of fluidic actuation, exploring the benefit of nano-
63 engineered surface and etc.

64 In this study we, for the first time, report on the fabrication and characterization of a microfabricated
65 electrokinetic biosensor and a chip manifold for easy integration of the microchips with standard fluidic
66 connections. The microchannels were fabricated on Si substrate followed by anodic bonding with glass
67 to achieve high surface quality as well as robust and transparent fluidic channels. The channels were
68 characterized to have low surface roughness and uniform cross section along the length. The devices
69 show linear and highly reproducible values for flowrate and streaming current with a standard deviation
70 below 5 pA, as a function of applied pressure. The microchips designed for multiplexed measurements
71 were tested with the detection of free proteins (streptavidin) and also transmembrane proteins of small
72 extracellular vesicles (sEVs) to demonstrate the capacity to detect various types of bio-analytes. The
73 limit of detection (LOD) for streptavidin was estimated to be 0.5 nM while for the transmembrane
74 protein (CD9), the LOD was found to be 1.2×10^{6} sEVs/mL. The sensitivity (LOD) of the devices were
75 improved by about 60% in case of streptavidin and 4-fold for CD9 targeted sEVs, when compared to
76 commercial silica capillary [9]. The improvement in LOD is attributed to a higher density of surface
77 charges which may be further exploited for even lower LOD. In addition, the chip manifold and the
78 microchip are equipped with optical window and a transparent glass to utilize optical detection of the

79 captured targets. The development of highly sensitive and reusable electrokinetic microchip-biosensor
80 is expected to take the sensing principle one step closer to clinical applications in the near future.

81 ## 2. Materials and Methods

82 ### 2.1. Reagents

83 For the study we used ultra-pure deionized water (resistivity: 18 MΩ. cm) locally produced. Phosphate
84 buffered-saline tablets, avidin from egg-white, streptavidin from *Streptomyces avidinii* were purchased
85 from Sigma Aldrich Sweden AB. For cleaning of the chips, hydrogen peroxide and ammonium
86 hydroxide were used which were also procured from Sigma Aldrich Sweden AB. The capturing probes
87 consist of Poly(L-lysine)-graft-biotinylated PEG (PLL-g-PEG-biotin) were purchased from Nanosoft
88 Polymers. Biotinylated human Anti-CD9 (MEM-61) (catalog no. MA1-19485) antibody and mouse
89 IgG1 isotype control (catalog no. IC002B) antibodies were purchased from Thermofisher Scientific and
90 Bio-Techne, UK, respectively.

91 ### 2.2. sEVs isolation, collection, and characterization

92 In this study sEVs were isolated from cell culture media of the non small-cell lung cancer (NSCLC)
93 cell line H1975 (ATCC® CRL-5908™, LGC Standards, Wesel, Germany). The cells were cultured in
94 RPMI-1640 medium with addition of fetal bovine serum (FBS, 10%) and 2 mM L-glutamine (Gibco,
95 Life Technologies, Stockholm, Sweden). sEVs were isolated from 50 mL of cell culture media with
96 two steps of centrifugation to clear out cell debris (200 RCF for 5 min followed by centrifugation of
97 supernatant at 720 RCF for 10 min, Rotina R38 centrifuge, Hettich). Media was concentrated to about
98 500 µL using Amicon Ultra-15 Centrifugal Filter Unit with a MWCO of 3 kDa (#UFC900324, Merck
99 Chemicals and Life Science AB, Solna, Sweden). sEVs were isolated by size-exclusion
100 chromatography (SEC) on qEVoriginal columns (Izon Science, Oxford, UK) as previously described
101 [12]. Briefly, the samples were added to the column and were eluted in 500 µL fractions by 0.22 µm
102 filtered PBS. Fractions 6-10 were pooled and concentrated to about 500 µL using an Amicon® Ultra-4
103 Centrifugal Filter Unit (#UFC800324, Merck Chemicals and Life Science AB). The particle size and
104 zeta potential were characterized by nanoparticle tracking analysis (NTA, Zetaview from particle

105 Metrix). For these analyses the sEVs samples were diluted 1:1000 in filtered PBS. The sample was
106 injected in 100 µL portions for three times and the cell temperature was maintained at 24ºC. The size
107 analysis was done on eleven positions in the sample cell while for the zeta potential a two-position
108 measurement was performed.

109 **2.3. Surface functionalization**

110 The exposure of the active surface of the sensor to the air as well as the chemical processes during the
111 fabrication decrease the quality of the surface oxide. Hence, prior to the antibody/receptor
112 immobilization, the surface of the microchannels were cleaned using RCA1 (5:1:1 DI-Water:
113 H_2O_2:NH_4OH) cleaning solution at 88°C for 30 minutes. In this process, atomic layers of silicon dioxide
114 on top are etched away by the diluted ammonium hydroxide and a fresh layer of silicon dioxide is
115 created by the hydrogen peroxide solution. Supplementary Information S1 demonstrates the effect of
116 the cleaning process on the recorded streaming current.

117 After the RCA1 cleaning process, the surface hydroxyl groups on the microchannel are activated
118 leading to a larger negative surface charge density. For the antibody/receptor immobilization, we
119 followed an optimized strategy as reported in our earlier work [8]. In brief, the surface of the
120 microchannels were first coated with a thin layer of PLL-g-PEG-biotin (PPB) by flowing an aqueous
121 solution (0.1 mg/mL) of PPB through the microchannels for 30 minutes. For the detection of
122 streptavidin, PPB layer was directly used where biotin of PPB layer acts as the receptor (Figure 1a).
123 For the control measurements, the surface of the sensor was covered by high concentration of
124 streptavidin (500 nM) using PPB. Then different concentrations of streptavidin were injected into the
125 devices to measure the background signal as the control.

126 In the case of membrane protein profiling of sEVs, CD9 tetraspanin was targeted. In that case,
127 biotinylated antibodies for CD9 were conjugated to the PPB coated surface using avidin as a linker
128 molecule. For the control measurements, mouse IgG1 isotype control antibody was used instead of the
129 specific capture antibody, i.e. anti-CD9. The concentration of the capture/control antibody was 50
130 μg/mL in 1xPBS and was immobilized for 1 hour. Prior to the sensing measurements, the microchannels

were treated with pluronic (synperonic) F108 solution for 20 minutes in order to suppress non-specific binding.

2.4. The measurement setup and the microchip

The experimental setup, shown in Figure 1b, consists of a high-pressure pure nitrogen gas capsule regulated by an Elveflow OB1 flow controller coupled with a thermal time of flight (TOF) flow sensor (Elveflow, MSF3) to measure the flowrate during the experiments. The working fluids (either the bio-sample or the analyte) are hydraulically pushed by the nitrogen gas into the system through PEEK tubing and microfluidic connections procured from Darwin Microfluidics, France. A continuous train of trapezoidal pressure pulses between 1.5 and 3 bar, having a pulse duration of 30 s was used in the method in order to perform a two-points streaming current measurement. The currents were measured using hollow Platinum tube electrodes placed at the inlet and outlet ports. The resulting streaming current pulses (ΔI_s) were measured by a Keithley picoammeter (model no. 2636A) while the pressure pulses (ΔP) were recorded directly by the pressure regulator.

The measured streaming current (I_s) by the electrodes was used to calculate the apparent zeta potential (ζ^*) of the microchannel surface using Eq. 1 [13].

$$\zeta^* = \frac{\eta}{\varepsilon\varepsilon_0}\frac{\Delta I_s}{\Delta P}\frac{L}{A} \qquad (1)$$

where η and $\epsilon\epsilon_0$ refer to the dynamic viscosity and permittivity of the measurement buffer, respectively, and L and A refer to the length and cross-sectional area of the microchannels, respectively. More details on the working principle could be found in our previous report [11].

In this study, we performed both real-time and endpoint measurements. The end-point measurements involved recording the initial baseline (ζ_i^*) and the final baseline after the injection of the sEVs ($\zeta_i^* + \Delta\zeta^*$). The injection of sEVs was done in 1x PBS to maintain the physiological conditions for the sEVs, whereas both the baselines were measured in 0.1x PBS to reduce the electrostatic screening. A Labview

153 program recorded the data, and a custom Python script was used to analyze them afterwards. The noise-
154 sensitive components of the experimental setup were placed in a Faraday cage to minimize the exterior
155 perturbation on the measurements. The heart of the assembled system is a custom-built manifold
156 platform to mount the biosensor chip and to ensure a leak-proof interfacing with standard fluidic
157 connectors even at high pressure (up to 6 bar). For this purpose, an octagonal-shaped PEEK block was
158 machined, on the center of which the microchip was placed. Suitable holes are drilled in the block with
159 the same diameter as the inlet/outlet ports on the biosensor. In order to eliminate the leakage from the
160 system, silicone rubber o-rings, purchased from Apple Rubber Inc., the USA, with 1 mm inner diameter
161 were placed between the biosensor and the platform, and finally two plastic plates were used to
162 sandwich the microchip on the platform. An optical window was designed on the plastic holders in
163 order to perform fluorescence microscopy. Figure 1c shows the cross-sectional view of the chip
164 platform along with the microchip. The silicon and glass substrates were purchased from
165 MicroChemicals Company, Germany. Other required material and devices for the microfabrication
166 were provided by Myfab, the Swedish research infrastructure for microtechnology, nanoscience and
167 materials research.

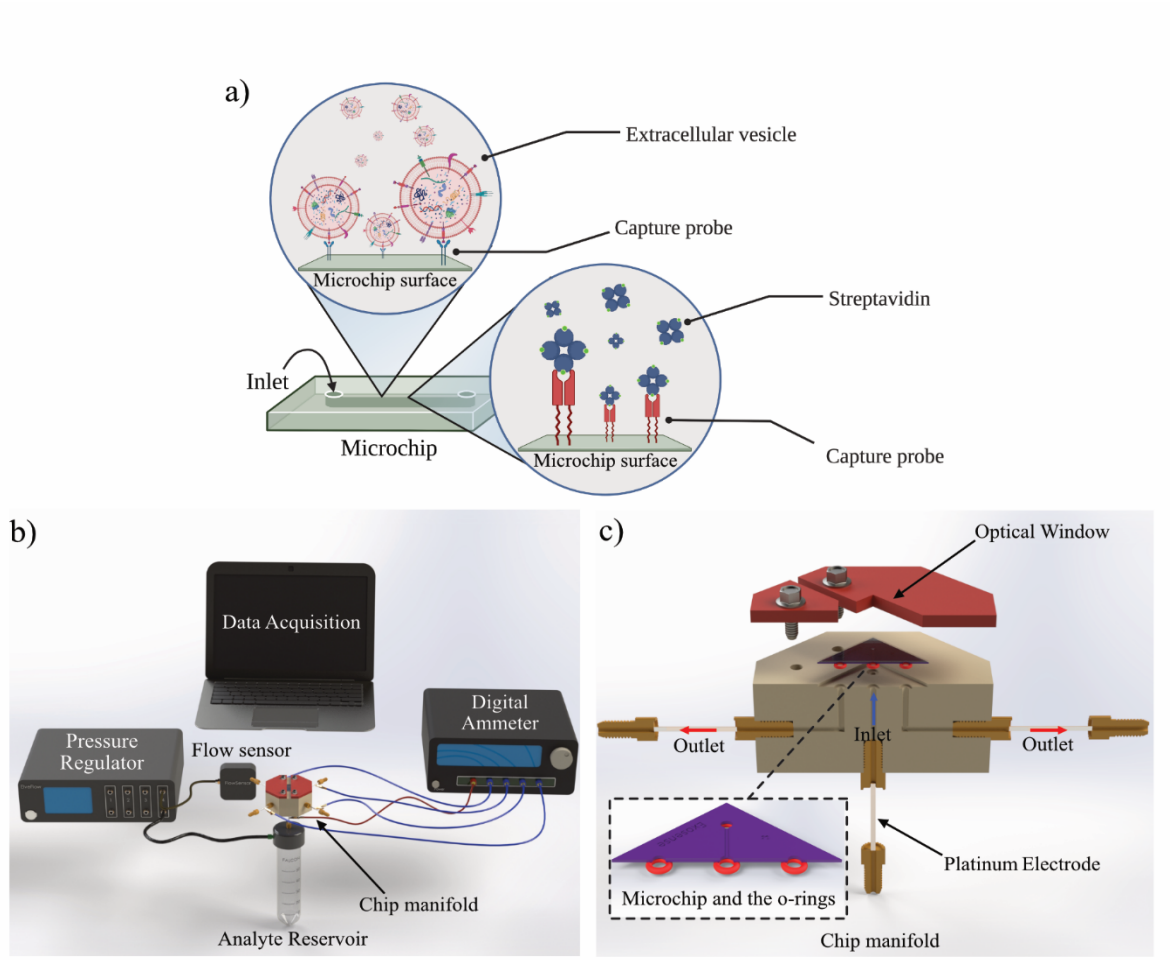

Figure 1 – a) Functionalization technique of the capture probes and the target, b) The schematic of the experimental setup consisting of the chip holder platform, platinum electrodes, digital ammeter, pressure regulator, flow sensor, analyte reservoir, and data acquisition system, c) The cross sectional view of the chip manifold and the microchip

3. Results

The devices are based on silicon-glass microfluidics where the microchannels of rectangular cross section were etched on Si substrate using reactive ion etching followed by an anodic bonding with thin quartz glass for sealing the channels. Typical dimensions of the fabricated channels are 10 µm × 25 µm in cross section and 3 mm in length. A schematic step by step procedures for the microchip processing and the final product are shown in Figure 2a and b, respectively. For the fabrication, a 100 nm thick layer of aluminum was sputtered on a 4 inch <100> single-side polished silicon wafer. This was followed by a coating of 500 nm thick layer of S1813 photoresist by spin coating and a soft baking at

110°C for 2 minutes. The sensor patterns were generated on the surface through the first lithography. After the development and hard baking of the resist at 120 °C for 10 minutes, the thin aluminum mask was dry etched so that the sensor pattern appears on the substrate. Thereafter, a 10 µm deep reactive ion etching of the silicon wafer was performed that forms the general geometry of the sensor (Figure 2a-1). After washing the aluminum mask off the substrate by wet chemistry, a new 300 nm thick protective aluminum layer was deposited on both sides of the silicon wafer. To create the inlet and outlet ports, the silicon wafer must be etched through. The bottom aluminum protective layer prevents helium leakage during the dry etching in the DRIE machine. A second photomask was used to pattern the inlet and outlet ports on the wafer. Thereafter, a dry etching of the aluminum protective layer (Figure 2a-2) followed by a deep dry etching of the silicon wafer was done (Figure 2a-3). After washing off the protective layers on the silicon wafer using wet chemistry, the substrate underwent a standard RCA surface preparation. Finally, a 300 nm thick layer of dry silicon dioxide was thermally grown on the substrate acting as the active sensing surface.

As the last step of the microfabrication, the substrate underwent a piranha cleaning process prior to the anodic bonding with a borofloat glass wafer (Figure 2a-4). The final product was diced using a high-speed rotary saw into 12 mm × 12 mm devices for the experiments. More details of the fabrication process flow could be found in the supplementary information S2.

Figure 2b shows a fully processed wafer containing 34 chips (left) and also finger-tip size single microchip (12x12 mm) containing four identical channels with a common inlet (at the center) and separate outlets. The geometry of the microchip and surface roughness of the fabricated devices were characterized using white light interferometry (WLI) method. For this purpose, an unbonded device was cleaned using RCA 1 cleaning solution and the structure was characterized by ZYGO optical profiler (Nexview NX2). Furthermore, the roughness elements were analyzed individually at different locations. Figure 2c shows the roughness of the surface. A total number of about 340K data points were analyzed and the centerline average was 9 nm.

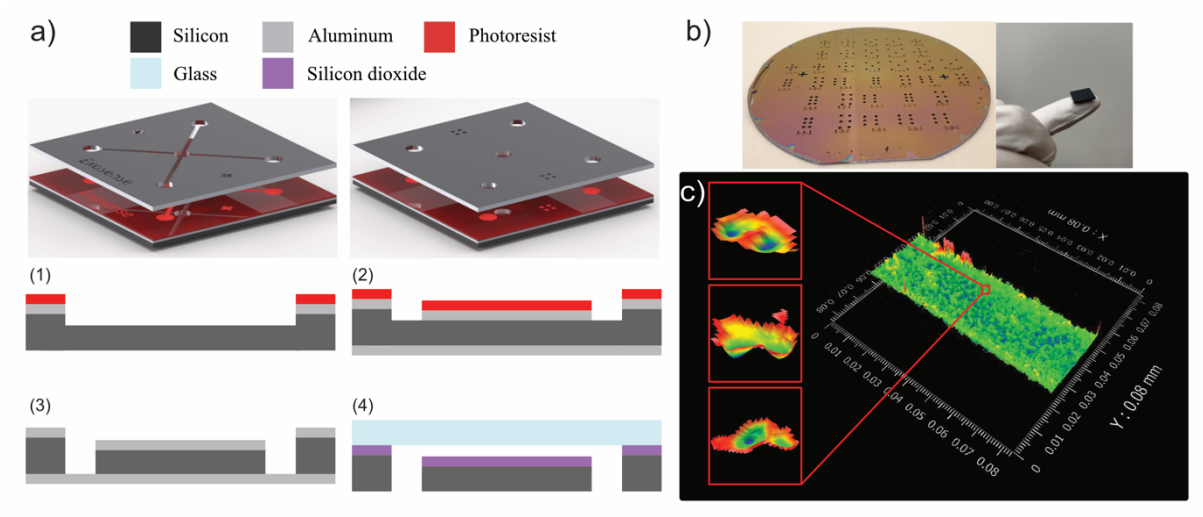

Figure 2 – a) the schematic of the device microfabrication process flow, b) a full wafer prior to bonding and dicing as well as the size scale of the final product, c) Roughness elemental analysis to calculate the mean of the roughness elements

3.1. Electrical and fluidic characterization

To shed light on the noise characteristics of the fabricated biosensor, streaming current was measured by flowing 0.1xPBS through a set of cleaned microchannels at different upstream pressures ranging between 1 and 6 bar. The RMS noise was calculated and is presented in Figure 3a as bar plots for different upstream pressures. Clearly, the RMS noise increases with increasing applied pressure and streaming current. The distribution of noise is shown in the inset of Figure 3a. As seen, the RMS noise remains similar (7 pA with standard deviation below 2 pA, n=3) up to 3 bars of applied pressure but then sharply increases, reaching 21 pA at 6 bars. The noise RMS at 3 bar corresponds to 0.42 mV of zeta potential which we defined as the minimum detectable signal (MDS) for the microchip sensor. Figure 3b shows the volumetric flowrate and streaming current measured in a cleaned microchannel as a function of the applied pressure. As expected, both the current and the flow rate show a linear and highly reproducible dependence on the applied pressure. The linear relation between upstream pressure and the measured flowrate with negligible deviation clearly indicates that both the microchip and the chip manifold are leak-proof within the measured pressure range. A simple Poiseuille estimation of the flowrate is also shown in Figure 3b which demonstrates a negligible deviation of the experimental

flowrate from the theoretical predictions. The error bars correspond to 3 measurements on different microchips with the same production method.

In order to characterize the flow regime in the microchannel, the Reynolds number was calculated for different applied upstream pressures ranging from 1 to 6 bar (see section S3). Decreasing the size of the microchannels and consequently increasing the surface to volume ratio projects the wall effect on the flow characteristics [14]. A proper model for friction factor calculation could help compare the experimental data and the theoretical predictions to estimate the wall effects. The pressure drop estimation is also an important parameter in fluidic characterization of the system. Therefore, different fluidic components were analyzed, and the estimated pressure drops were calculated (see section S4).

Eventually, a stable and identical flow rate through all the microchannels need to be established as the devices are design for multiplex sensing. For the purpose of this study, a flow sensor was placed at the common inlet and the flowrate was measured at 3 bars. Then, channel 1 (C1) was blocked using microfluidic blockers at the outlet of the chip manifold and the flowrate was measured. The same process was repeated by blocking other two channels consecutively. Since the channels are expected to operate in an identical way, a negligible difference in flowrate is required when the sample is injected through a common inlet. The flowrate measurement data at each microchannel is shown in the section S5. The standard deviation of the flowrates at different microchannels is 96 nL/min while the average flowrate is 13 μL/min at 3 bar of upstream pressure. Blocking microchannels and measuring the flowrate at the others would show a clear picture of the fluidic crosstalk valuable for future multiplex biosensing. In addition, it is vital to know that a possible blockage in one channel during the experiments would not lead to the failure and/or deviation of the sensing results in the other microchannels. The standard deviation of the flowrate at different microchannels demonstrate a negligible fluidic crosstalk and effect of the blockage in other channels.

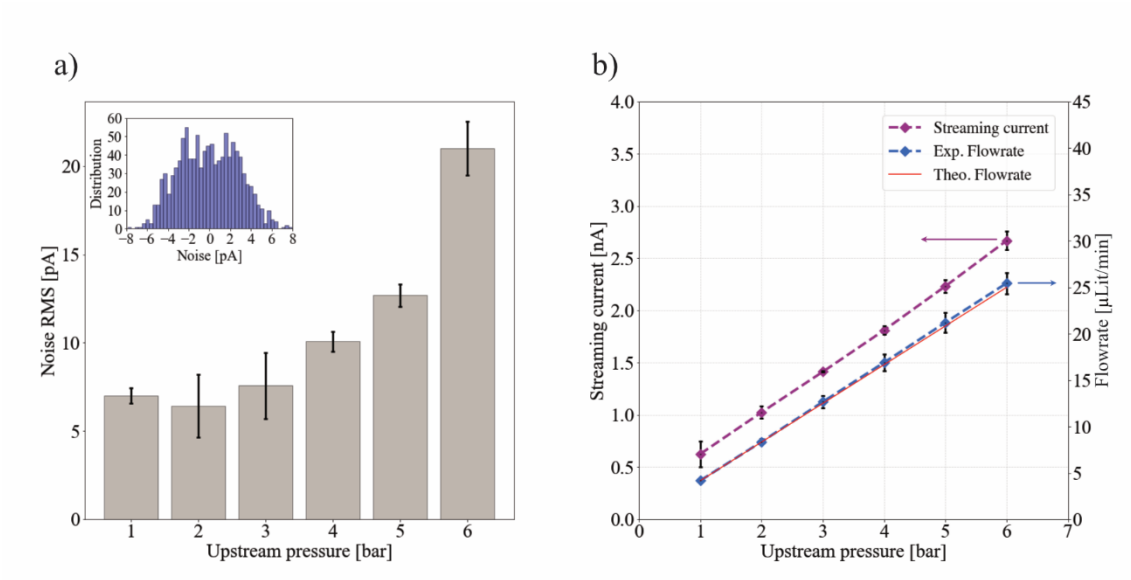

Figure 3 – a) Root mean square of the noise at different upstream pressures along with the noise distribution, b) linear relation between the flowrate and streaming current versus the upstream pressure

3.2. Sensing performance

The sensing performances of the devices were first investigated using a well-studied protein-ligand pair, i.e. biotin-streptavidin. Figure 4a shows a set of real-time measurements for two concentrations of streptavidin injected to PPB coated microchannels. For the detection measurement, the zeta potential of the PPB coated surface was first measured (baseline) by injecting 0.1x PBS, until a stable baseline was obtained. Thereafter, streptavidin dissolved in 0.1x PBS was injected and the real-time data was recorded for 1 hour of injection. The results are shown in Figure 4a. As can be seen, the microchip surface reaches an equilibrium in less than 20 minutes for higher concentrations while it takes over 40 minutes at a lower concentration. In order to compare the results with previously used commercial microcapillary-based sensor, a set of end-point streptavidin measurements under identical conditions were performed for both microchip and capillary. For this purpose, a 4 cm long capillary tube with an inner diameter of 25 µm was used. The microcapillaries were cleaned and functionalized using an identical procedure as described earlier. Figure 4b shows a comparison between the signals obtained with a microchip and a microcapillary based system. The measurements were performed for different concentrations of streptavidin ranging from 10 pM to 100 nM in order to evaluate the limit of detection in the two cases. As seen, the signal, measured in terms of apparent zeta potential, proportionally

264 increases from 1.72 mV to 10.25 mV for the microchip. At all of the concentrations, the microchip-
265 based sensor demonstrated higher sensitivity with an enhanced signal over the capillary-based sensor.
266 In addition, comparing the error bars of two systems, microchip-based sensing seems more reproducible
267 in comparison to capillary-based sensing. To further analyze the data and to demonstrate another
268 potential advantage of having a transparent window in the channel design, the fluorescence signal
269 arising from the Atto 565 conjugated streptavidin binding to the channels were also recorded. The
270 images are shown in Figure 4c. As can be seen, the fluorescence intensity scales with the concentrations
271 as expected. In addition, the control channel shows no/negligible fluorescence signal indicating a good
272 specificity of the detection. For comparison of the detection sensitivity between the microchip and
273 capillary-based sensing, we estimated the limit of detection (LOD) by a linear fit of the concentration
274 vs signal (calibration) curve thus obtained (Figure 4b and supplementary information S6). The LOD
275 was determined as the concentration of the target corresponding to the MDS of the sensor. The MDS
276 of the microcapillary and microchips are 0.2 mV and 0.4 mV, respectively. The MDS of the microchip
277 is slightly higher as compared to microcapillary. This observation is because of having four
278 interconnected microchannels in microchips while for the microcapillary, a two-microchannel
279 configuration was used. This observation is inline with the previous work of our group [10]. The LOD
280 estimated for the microchip and microcapillary based systems was 0.5 nM and 0.8 nM, respectively.
281 The indicated data points at the lowest concentration were out of the dynamic range of the sensor that
282 are not considered for LOD calculation.

283 Beyond protein detection, streaming current-based sensor has also been investigated for the detection
284 and surface protein profiling of sEVs [5, 10], an emerging bio-analyte which is attracting a significantly
285 growing interest both for diagnostics and therapeutics [15]. A major advantage of streaming-current
286 based sensor for sEVs detection arises from its size-dependent sensitivity, as demonstrated in our
287 previous reports [11]. sEVs (diameter: 50-150 nm) being much larger than proteins can be detected
288 with a fM range detection sensitivity using the streaming current-based technique [9]. In order to
289 investigate the performance of the current microchip-based platform, we analyzed the detection
290 sensitivity of sEVs derived from H1975 lung cancer cell line. The sEVs were first characterized using

291 a nanoparticle tracking analyzer (NTA, Zetaview from particle Matrix) for their size and zeta potential
292 measurement as presented in Figure 4d, e. The mean diameter of the sEVs as well as their zeta potential
293 were measured to be 132 nm and -25.83 mV, respectively. The narrow distribution of the sEVs zeta
294 potential demonstrates the consistent signal after the detection of the sEVs across the experiments. The
295 sEVs were then detected by targeting their CD9 transmembrane protein using the microchip. Figure 4f
296 shows the barplots representing the signal as a function of different concentration of sEVs. A calibration
297 plot along with the MDS is shown in the supplementary information (S7). The LOD obtained in this
298 case was 1.2×10^{6} particles/mL, which is about 4 times lower than the results previously obtained with
299 the capillary based system [9]. Clearly, both for streptavidin and sEVs detection, the microchip-based
300 platform significantly outperforms the previously reported capillary-based system.

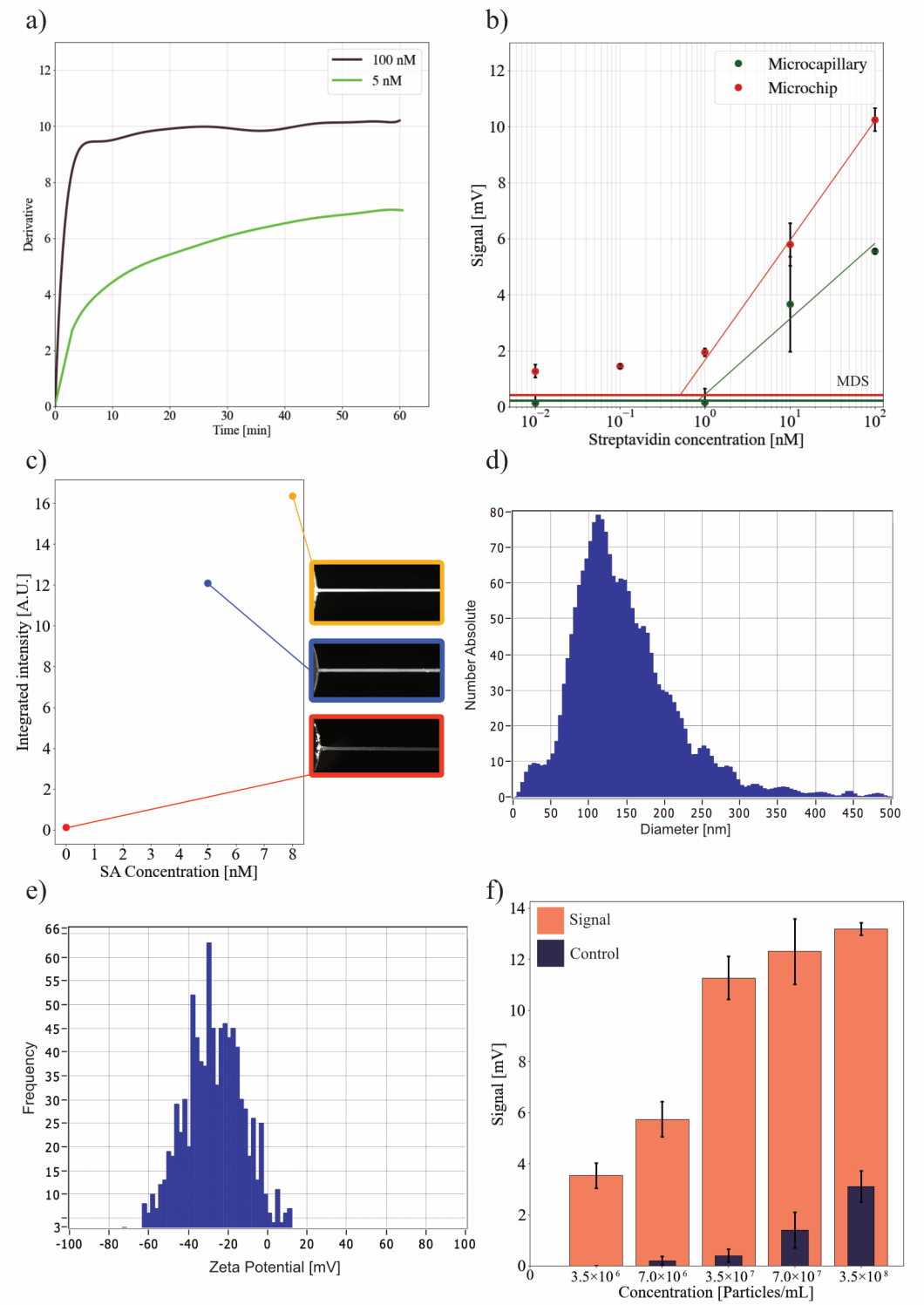

Figure 4 – a) Real time sensing of streptavidin using PPB as the capture probe in microchip with respect to time, b) Limit of detection comparison between microcapillary and microchip devices for end point streptavidin detection at different concentrations (controls were subtracted), c) Optical detection of fluorophore-tagged streptavidin captured by PPB in the microchip through the optical window, d) size distribution of the sEVs, e)

305 *zeta potential distribution of sEVs, f) Limit of detection for CD9 biomarker of H1975 derived sEVs at different*
306 *concentrations*

307 **4. Discussion**

308 The main contribution of the present study is the development of a microchip technology for the
309 streaming current-based detection of biological analytes. While the detection method has been widely
310 studied [2, 5, 9] and innovated during the past years, most of the research has been focused on the
311 fundamental principle and exploitation/optimization of the method aiming to achieve a better sensitivity
312 and specificity [9]. These studies have been done mainly using PDMS microchannel and/or commercial
313 silica microcapillaries. Nevertheless, these research efforts have considerably contributed in the
314 improvement of the method, thereby, extending the applicability of the method for the analysis of
315 various biological targets, e.g., proteins [2], DNA [16] and sEVs [5], as well as exploring different
316 diagnostic opportunities, e.g., the monitoring the efficacy of precision cancer medicine [10], albeit in a
317 laboratory setting. Translation of these technical developments for potential use in clinical setting is an
318 obvious next step which is the primary objective of the research presented here. In this context, the
319 development of a robust and easy-to-use setup is a key requirement along with the development of a
320 microchip that can be mass fabricated. Going further, the entire platform has been characterized for
321 electrical noise, fluidic and electrokinetic characteristics as well as sensitivity towards some common
322 biological targets. In addition, by comparing with a previously used commercial silica capillary, a clear
323 improvement in detection sensitivity has been demonstrated. Some of these aspects are further
324 discussed in the following section. To the best of our knowledge, such a platform has not been reported
325 until now and thereby constitutes the main novelty of the current work.

326 **The microchip and the detection platform**: The fabricated microchips clearly show high reliability
327 in the entire pressure range. This is evident from both the flow rate analysis of different chips and micro-
328 channels (Fig 3b and S6) and the streaming current measurement as a function of the applied pressure
329 (Fig 3b). The measurement of streaming current as a function of pressure shows a highly linear behavior
330 with a standard deviation ~ ±90 pA in the entire pressure range. Fig. 3b also indicates leak-free
331 integration of the chip with the manifold allowing easy interfacing with the commercial microfluidic

connectors. The choice of Si-glass microfluidics offers several other benefits, particularly in the context of streaming current based bio-detection. As reported earlier [9, 17], surface roughness can negatively impact the sensitivity of detection. With the optimization of the Si fabrication process, the roughness can be easily controlled. As shown, in Fig. 2c, the roughness of the fabricated channels stands at a mean value of 9 nm which is comparable to many antibodies. Secondly, the geometry can be precisely controlled with nanoscale precision and the anodically-bonded devices offers unparallel chemical compatibility and bonding strength [18]. Finally, SiO_2 surface has been widely studied for the immobilization of biological recognition molecules [19, 20] and there are well established protocols which allows highly reproducible surface functionalization.

Electrical and fluidic characteristics: There is a variety of sources introducing noise in the recorded data such as flow disturbance, electrical measurement system, ambient noise, microscopic fluctuations and impurities, and intrinsic sources. The conductive components of the experimental setup are accommodated inside a Faraday cage and the interior walls of the cage are covered by insulating tapes to avoid short circuit and electromagnetic noise. The RMS of the noise at different upstream pressures recommends low applied pressure for the measurements (between 1 and 3 bar). On the other hand, the two-point streaming current measurement requires two upstream pressures to form the desired waveform. For the upper value of the pressure 3 bar was nominated. However, for the lower value, 1.5 bar was chosen instead of 1 bar to ensure higher data sampling rate. Therefore, the RMS noise stays roughly the same for the range of the experiments. In addition, the low absolute value of streaming current leads to a negligible polarization of the electrodes as demonstrated above by the linear relation between the upstream pressure and the streaming current in the working range of the device.

The fluidic analysis on the other hand shows that the friction factor inside the microchip agrees with the analytical predictions. The pressure drop in the fluidic path due to multiple bends in the microchip manifold, different microfluidic connectors, inlet effects, and the electrovisous effect are studied for the current system (supplementary information S4) [11, 12].

Sensing performance: The sensitivity of the fabricated devices has been evaluated by detecting streptavidin at two and five concentrations for real-time and endpoint measurements, respectively. The

359 results presented in Figure 4a and b, show that the microchip biosensor is suitable for both real-time
360 and endpoint measurements in a broad range (10 pM to 100 nM). The LOD of the developed technique
361 in this study was compared with the commercial silica microcapillaries to show the improvement over
362 our previous data [9]. The calibration curves for both systems show 60% improvement in the limit of
363 detection for the microchip biosensor. In addition, the measurement uncertainty (standard deviation,
364 n=3) for the microchip biosensors are significantly lower as compared to that of the capillary biosensors.
365 On the other hand, the transparent microchips along with the chip manifold facilitates the optical
366 analysis of the target. The optical window on the chip manifold and its appropriate design for the optical
367 microscope sample holder makes it possible to optically analyze the targets in the microchannel. The
368 sensing performance of the platform was also evaluated with the profiling of sEV membrane proteins.
369 As mentioned earlier, an improvement in the detection sensitivity by a factor of 4 was also observed,
370 when compared to commercial microcapillary. The improvement can be attributed to a better surface
371 quality of the thermally grown SiO_2 surface. As demonstrated in our previous report, surface charge
372 density and electrostatic charge contrast play a critical role in determining the detection sensitivity. In
373 order to compare the surface charge densities, we cleaned a microchip and a capillary sensor using the
374 protocol explained earlier. Then measured the baseline. Thereafter, the same process was repeated after
375 PPB and CD9 antibody functionalization.

376 Better surface coverage by the PPB layer would make a more positive surface that can attract more
377 negatively charged targets (streptavidin or sEVs). Therefore, on one hand having a negatively charged
378 surface at the pH of the buffer used for the experiments could enhance the surface coverage by the PPB
379 layer and on the other hand, a too negative surface could repel the negatively charged biomolecules
380 such as the sEVs. To demonstrate the mentioned tradeoff, the surface charge density of the microchip
381 is calculated and compared with the microcapillaries here.

382 The 1-dimentional solution of the Poisson-Boltzmann equation that governs the length of the EDL on
383 a charged surface, shows the relation between surface electrostatic potential and the surface charge
384 density. The effective surface charge density, on the other hand, could be calculated from the zeta
385 potential of the surface (Eq. (2)) [23].

$$\sigma_{eff} = \sqrt{8cN\varepsilon_r\varepsilon_0 k_B T}\sinh\left(\frac{e\zeta}{2k_B T}\right) \quad (2)$$

386 A better surface quality attracts more capture probes on the surface and makes a more positively charged
387 surface that can act in favor of attracting more negatively charged targets i.e., streptavidin and sEVs.
388 The effective surface charge density of the bare capillary and the microchip are -5.3×10^{-3} and $-5.6\times10^{-}$
389 ^{3} e/nm^2, respectively, showing higher density of the charges on the bare surface of the microchip as
390 compared to the capillary. After PPB functionalization, the effective charge density is -0.08×10^{-3} e/nm^2
391 for the microchip while it is -0.35×10^{-3} e/nm^2 for the capillary sensors. for the capillary sensors. These
392 numbers after the immobilization of CD9 antibody are -0.45×10^{-3} e/nm^2 and -0.9×10^{-3} e/nm^2 [9] for
393 microchip and capillary, respectively. This indicates a higher surface adsorption of the positively
394 charged PPB in case of the microchip, making the overall surface charge density less negative. This
395 better facilitates the sensing of the negatively charged sEVs and could explain the lower limit of
396 detection discussed before. The limit of detection for streptavidin and sEVs by CD9 surface protein
397 were 60% and 4 time better than that of the microcapillaries when compared under identical conditions,
398 respectively. Finally, the devices were cleaned using the RCA1 cleaning protocol. The results
399 (supporting information S8) show that the baseline could be recovered up to five times after the
400 experiments promising a sustainable detection platform.

401 **5. Conclusion**

402 In this study, a microfluidic device was fabricated out of silicon and was covered by a thin layer of
403 silicon dioxide as the active surface of the biosensor. The hydroxyl groups on the surface carrying
404 negative charge were activated by wet chemistry to attract Ploy-L-Lysine molecules conjugated with
405 PEG and biotin on the surface acting as the capture probes for the biosensing. A robust experimental
406 setup was designed and assembled to facilitate electrical measurements as well as a leak-proof fluidic
407 path for the experiments. The zeta potential of the microchannel inner surface was calculated using
408 streaming current measurements during the experiments. The zeta potential of the surface before and
409 after capturing a specific target is the sensing signal in this study. The measured noise of the fabricated
410 biosensor was characterized by calculating root mean square at different upstream pressures from 1 to

411 6 bar. Upstream pressures of 1.5 and 3 bar were chosen as the working condition for the experiments.
412 The linear relation between the upstream pressure and the measured streaming current/flowrate was
413 controlled as well as the fluidic crosstalk between the microchannels. Thereafter, the performance of
414 the microchip-based biosensor was compared with commercial microcapillary tubes. The sensitivity of
415 the microchip device was one order of magnitude higher, and they showed reusability after the
416 experiments. Finally, CD9 surface biomarker of the extracellular vesicles from H1975 cell line were
417 captured specifically by the capture probes immobilized on the surface. The calibration curves show a
418 1.2×10^6 particle/mL detection limit for the microchip biosensor.

419 In conclusion, we could demonstrate the successful replacement of microcapillary tubes with
420 microchip-based biosensors working with streaming current measurement. The results showed a faster,
421 more sensitive, more robust, and reusable substitution to the commercial microcapillary tubes for
422 biosensing applications.

423 **Conflict of interest**

424 The authors declare no conflict of interest.

425 **Acknowledgement**

426 This study was supported by grants from the Swedish Research Council (grant no. 2016-05051), the
427 Erling Persson Family Foundation, Stockholm Cancer Society (#171123, #191293, and #201202), the
428 Swedish Cancer Society (CAN 2015/401; CAN 2018/597), Stockholm County Council (#20160287
429 and #20180404), and funds of Karolinska University Hospital FOUU (#75032). Dr. Örjan Vallin and
430 Dr. Milena De Albuquerque Moreira are acknowledged for their input in the microfabrication steps.

431 **References**

432 [1] C. Glad, K. Sjödin, and B. Mattiasson, "Streaming potential—a general affinity sensor," *Biosensors*,
433 vol. 2, no. 2, pp. 89–100, 1986.
434 [2] A. Dev *et al.*, "Electrokinetic effect for molecular recognition: A label-free approach for real-time
435 biosensing," *Biosens. Bioelectron.*, vol. 82, pp. 55–63, 2016.
436 [3] J. O. Lee, N. Choi, J.-W. Lee, S. Song, and Y.-P. Kim, "Rapid electrokinetic detection of low-

437 molecular-weight thiols by redox regulatory protein-DNA interaction in microfluidics," *Sensors*
438 *Actuators B Chem.*, vol. 336, p. 129735, 2021.
439 [4] Y. Li, S. N. Lai, and B. Zheng, "A microfluidic streaming potential analyzer for label-free DNA
440 detection," *Sensors Actuators B Chem.*, vol. 259, pp. 871–877, 2018.
441 [5] S. Cavallaro *et al.*, "Label-free surface protein profiling of extracellular vesicles by an electrokinetic
442 sensor," *ACS sensors*, vol. 4, no. 5, pp. 1399–1408, 2019.
443 [6] D. Lupa, M. Oćwieja, N. Piergies, A. Baliś, C. Paluszkiewicz, and Z. Adamczyk, "Gold nanoparticles
444 deposited on silica microparticles-Electrokinetic characteristics and application in SERS," *Colloid*
445 *Interface Sci. Commun.*, vol. 33, p. 100219, 2019.
446 [7] H. Qi *et al.*, "Rapid detection of trace Cu2+ using an l-cysteine based interdigitated electrode sensor
447 integrated with AC electrokinetic enrichment," *Electrophoresis*, vol. 40, no. 20, pp. 2699–2705, 2019.
448 [8] S. S. Sahu *et al.*, "Electrokinetic sandwich assay and DNA mediated charge amplification for enhanced
449 sensitivity and specificity," *Biosens. Bioelectron.*, vol. 176, p. 112917, 2021.
450 [9] S. S. Sahu *et al.*, "Exploiting Electrostatic Interaction for Highly Sensitive Detection of Tumor-Derived
451 Extracellular Vesicles by an Electrokinetic Sensor," *ACS Appl. Mater. Interfaces*, 2021.
452 [10] S. Cavallaro *et al.*, "Multiplexed electrokinetic sensor for detection and therapy monitoring of
453 extracellular vesicles from liquid biopsies of non-small-cell lung cancer patients," *Biosens. Bioelectron.*,
454 vol. 193, 2021, doi: 10.1016/j.bios.2021.113568.
455 [11] S. S. Sahu, C. Stiller, S. Cavallaro, A. E. Karlström, J. Linnros, and A. Dev, "Influence of molecular
456 size and zeta potential in electrokinetic biosensing," *Biosens. Bioelectron.*, vol. 152, p. 112005, 2020.
457 [12] C. Stiller *et al.*, "Detection of tumor-associated membrane receptors on extracellular vesicles from non-
458 small cell lung cancer patients via immuno-PCR," *Cancers (Basel).*, vol. 13, no. 4, p. 922, 2021.
459 [13] R. J. Hunter, *Zeta potential in colloid science: principles and applications*, vol. 2. Academic press,
460 2013.
461 [14] M. Bahrami, M. M. Yovanovich, and J. R. Culham, "Pressure drop of fully developed, laminar flow in
462 rough microtubes," 2006.
463 [15] N. A. Hanjani *et al.*, "Emerging role of exosomes as biomarkers in cancer treatment and diagnosis,"
464 *Crit. Rev. Oncol. Hematol.*, vol. 169, p. 103565, 2022.
465 [16] D. C. Martins, V. Chu, D. M. F. Prazeres, and J. P. Conde, "Electrical detection of DNA immobilization
466 and hybridization by streaming current measurements in microchannels," *Appl. Phys. Lett.*, vol. 99, no.

18, p. 183702, 2011.

[17] Z. Adamczyk, K. Sadlej, E. Wajnryb, M. Nattich, M. L. Ekiel-Jeżewska, and J. Bławzdziewicz, "Streaming potential studies of colloid, polyelectrolyte and protein deposition," *Adv. Colloid Interface Sci.*, vol. 153, no. 1–2, pp. 1–29, 2010.

[18] Z. Qi *et al.*, "Disposable silicon-glass microfluidic devices: precise, robust and cheap," *Lab Chip*, vol. 18, no. 24, pp. 3872–3880, 2018.

[19] F. Nessark *et al.*, "Capacitance Polypyrrole-based Impedimetric Immunosensor for Interleukin-10 Cytokine Detection," *Electroanalysis*, vol. 32, no. 8, pp. 1795–1806, 2020.

[20] L. Jorde, Z. Li, A. Pöppelwerth, J. Piehler, C. You, and C. Meyer, "Biofunctionalization of carbon nanotubes for reversible site-specific protein immobilization," *J. Appl. Phys.*, vol. 129, no. 9, p. 94302, 2021.

[21] M. Akbari, D. Sinton, and M. Bahrami, "Pressure drop in rectangular microchannels as compared with theory based on arbitrary cross section," *J. Fluids Eng.*, vol. 131, no. 4, 2009.

[22] M. Bahrami, M. M. Yovanovich, and J. R. Culham, "Pressure drop of fully-developed, laminar flow in microchannels of arbitrary cross-section," in *International Conference on Nanochannels, Microchannels, and Minichannels*, 2005, vol. 41855, pp. 269–280.

[23] Z. Ge and Y. Wang, "Estimation of nanodiamond surface charge density from zeta potential and molecular dynamics simulations," *J. Phys. Chem. B*, vol. 121, no. 15, pp. 3394–3402, 2017.